# Control of Variable Geometry Turbocharged Diesel Engines for Reduced Emissions

A.G. Stefanopoulou[‡1] I. Kolmanovsky[**]
J.S. Freudenberg[+2]

[‡] Department of Mechanical and Environmental Engineering, UC, Santa Barbara, CA 93106

[**] Ford Research Laboratory, Ford Motor Company, Dearborn, MI 48121

[+] Department of Electrical Engineering and Computer Science, University of Michigan, Ann Arbor, MI 48109

**Abstract**

A multivariable control scheme is designed to minimize emission of nitrogen oxides ($NOx$) and generation of smoke in a Diesel engine equipped with a variable geometry turbocharger (VGT) and an external exhaust gas recirculation system (EGR). Steady-state optimization results in operating points where NOx emissions and smoke generation are highly coupled and require joint management by VGT and EGR actuators.

## 1 Introduction

In this paper we consider an automotive control problem for a variable geometry turbocharged (VGT) compression ignition direct injection (CIDI) engine with an external exhaust gas recirculation system shown schematically in Fig. 1. The

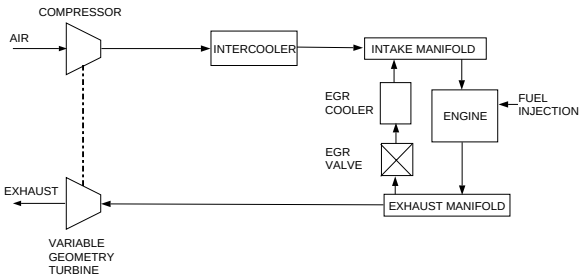


**Figure 1:** Schematic representation of the Diesel (CIDI) engine.

turbine converts energy of the exhaust gas into mechanical energy of the rotating turboshaft that, in turn, drives the compressor. The compressor increases the density of air supplied to the engine; this larger mass of air can be burnt with a larger quantity of fuel thereby resulting in a larger torque output as compared to (non-turbocharged) naturally aspirated engines [13]. The power generated by the turbine depends on the pressure and temperature of the exhaust gas and on the mass flow rate of the exhaust gas through the turbine. A turbine with variable geometry uses inlet guide vanes (located on the turbine stator) to modify its effective flow area and provide a better match between the turbocharger and the CIDI engine [7]. Through changes in inlet guide vane positions, the power transfer to the turbine and, hence, to the compressor can be modified and the airflow to the intake manifold can be controlled. For example, if the EGR valve is closed, closing the vanes results in a smaller turbine effective flow area, higher exhaust manifold pressure, increased power generation by the turbine and increased flow of air from compressor into the intake manifold. Opening the vanes produces the opposite effect.

To reduce the emissions of harmful oxides of nitrogen ($NO_x$) a portion of the exhaust gas can be diverted back to the intake manifold to dilute the air supplied by the compressor. This process is referred to as exhaust gas recirculation (EGR). It is, typically, accomplished with an EGR valve that connects the intake manifold and the exhaust manifold (See Figure 1). In the cylinders the recirculated combustion products act as inert gas thus lowering the flame temperature and, hence, decreasing the formation of $NO_x$ [4]. A high level of burned gas fraction, $F_1$, on the other hand, reduces the speed of response of the fresh air dynamics into the intake manifold and the cylinder [6]. This behavior is caused by the two distinct mechanisms by which EGR interacts with the fresh air flow into the cylinders. First, burned gas fraction from the EGR valve displaces fresh air from the intake manifold and consequently decreases the speed with which fresh air mass flows into the cylinders. Secondly, a fraction of the exhaust gas that can be used by the turbine is diverted through the EGR valve to the intake manifold, reducing the turbine power and consequently the flow delivered to the intake manifold through the compressor. Slow air flow dynamics coupled with a high dilution level can lead low in-cylinder air-to-fuel ratio ($AFR$), and consequently, unacceptable smoke generation. It is evident that the EGR system is associated with an inherent performance tradeoff between $NO_x$ and smoke generation. In particular, we show that the need to prevent smoke generation will limit our ability to reduce $NO_x$ emissions.

In this paper, we first derive a strategy to generate optimal setpoints for $F_1$ and $AFR$ as a function of fueling rate ($W_f$) and engine speed ($N$). Specifically, using a nonlinear sim-

[1] Work was accomplished while the first author was at Powertrain Control Systems Dept., International and Systems Laboratory, Ford Motor Company.

[2] Support is provided by the National Science Foundation under contract NSF ECS-94-14822; matching funds to this grant were provided by Ford Motor Company.

ulation engine model we choose operating points with the maximum value of $F_1$ possible given that $AFR$ must remain above an acceptable level to limit smoke. Our next step is to develop a control strategy with the goal of regulating the performance variables to the desired setpoints in response to changes in fuel command and engine speed. The regulation scheme will be based on measuring mass air flow and absolute pressure in the intake manifold. Two issues arise in the design of this control algorithm. First, the fact that we have optimized the performance variables implies that the desired setpoints tend to lie on the boundary of the set of feasible engine operating points. As a consequence, relatively small errors in the strategy will tend to generate infeasible setpoints. Second, at the desired setpoints, the $VGT$ and $EGR$ actuators do not have the authority to regulate $AFR$ and $F_1$ independently. The latter fact manifests itself in that the DC gain matrix of the plant is almost rank deficient. To address these issues, we analyze the directional properties of the plant using the singular value decomposition of the plant DC gain matrix [3]. We consequently gain-schedule a set of linear controllers that coordinate the actuators to achieve maximum authority and to reduce the impact of strategy errors. The achieved performance is demonstrated by using simulations and experiments.

## 2 Engine Model

In this section we summarize the engine model used in this study (see [6, 9] for a complete description of the model). It is derived using mean value engine modeling approach that assumes temporal and spatial averages of relevant temperatures, pressures and mass flow rates [1, 5, 12]. We treat engine speed as a slowly time-varying parameter. The engine model has nine states. The six states, $m_1$, $F_1$, $p_1$, $m_2$, $F_2$, $p_2$ represent the gas dynamics in the intake manifold and the exhaust manifold. Specifically, $p$ stands for gas pressure (kPa), $m$ for gas mass (kg) and $F$ for burned gas fraction. The subscript 1 identifies the intake manifold and the subscript 2 identifies the exhaust manifold. The burned gas fractions, $F_1$ and $F_2$, are defined as the density fractions of the combustion products in their mixture with air for the intake manifold and for the exhaust manifold, respectively. These fractions account for both the amount of combustion products and the amount of air recirculated back to the engine. The seventh state is the turbocharger rotor speed, $N_{tc}$ (rpm). Hereafter, we assume stable inner loop controllers for the pneumatic EGR valve and VGT vane actuators and we include their closed loop behavior in the engine model. The closed loop dynamics are represented by a first order system which introduces two additional states: EGR valve position ($\chi_{egr}$), and VGT actuator position ($\chi_{vgt}$). Their scaled range is between 0 and 1, where the position of 0 is completely open and 1 is completely closed.

## 3 Performance Objectives

The system performance objective is to reduce $NO_x$ emissions and avoid visible smoke generation while maintaining fast engine torque response. Torque response in CIDI engines depends mostly on the fueling level, $W_f$, and engine speed, $N$, during lean operation ($AFR > 14.6$). We assume a simple fuel governor as a static map that determines the appropriate fueling level based on driver's pedal position and engine speed, $N$. Thus, the fueling rate, $W_f$ (kg/hr), and engine speed, $N$ (rpm), are treated as external inputs to the engine ($w$) and not as control signals. Figure 2 shows the input-output signal definition for the CIDI engine.

As discussed before, reduction of $NO_x$ emissions is achieved with high dilution of the air charge that corresponds to large values of $F_1$, the burnt gas fraction in the intake manifold. Visible smoke can be avoided by keeping the in-cylinder air-to-fuel ratio, $AFR$, sufficiently lean. Thus, we employ the engine variables, $AFR$ and $F_1$ as performance variables that we want to optimize at each operating point (see Figure 2).

Conventional sensors of mass air flow and manifold absolute pressure are used to measure the intake gas process. Specifically, we measure the intake manifold pressure ($p_1$, using a $MAP$ sensor), and the air flow through the compressor ($W_{c1}$, using a $MAF$ sensor) as depicted in Figure 2.

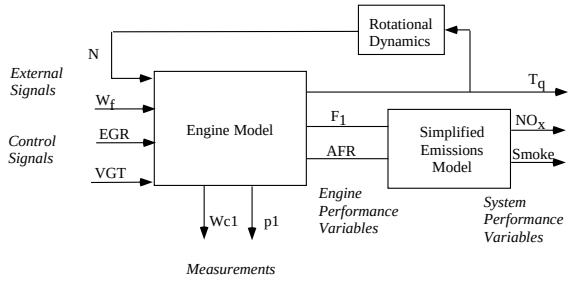


**Figure 2:** Signal definition for the CIDI control problem.

The fuel injection system in CIDI engines enables essentially instantaneous control of the fueling rate. Typically, rapid increases in fueling rate are limited to protect the driveline and to prevent smoke. In this work we are not addressing the design of the fuel limiter and we allow instantaneous increase of fueling rate in order to investigate the ability of $EGR$ and $VGT$ control in reducing $AFR$ excursions. Consider, temporarily, fixed $VGT$ and $EGR$ and an instantaneous increase in fueling rate. Utilizing the energy stored in the resulting exhaust gas the turbocharger will spin up to a new steady-state operating point and eventually increase the amount of air to the engine. Thus, changes in fueling rate cause a disturbance in $AFR$ which is partially rejected through the natural feedback that the turbocharger establishes between the engine exhaust and intake processes. It takes, however, a certain amount of time for the turbocharger to spin up and for the intake manifold to fill to a new level of pressure and air mass, thus, reaching a new equilibrium.

To summarize the input-output properties of the plant, changes in fueling rate affect rapidly the combustion process and the exhaust manifold. Furthermore, changes in fueling rate affect the intake manifold states primarily through the turbocharger, and secondly, through the open EGR valve. In point of fact, during fueling rate changes the performance variables, $AFR$ and $F_1$, and the measured variables, $W_{c1}$

and $p_1$, converge to a new equilibrium. This equilibrium and the transient trajectory, however, might not be the optimal with respect to the emission requirements and the time required to achieve convergence might be excessively long.

Our controller is designed to coordinate $EGR$ and $VGT$ to (i) speed up the engine open loop dynamics in order to reduce transient $AFR$ excursions, and (ii) to regulate $AFR$ and $F_1$ to a new optimum equilibrium. The resulting control problem is defined as follows:

$$\begin{array}{lll} \dot{x} & = f(x,u,w) & \text{State Equations} \\ y & = \left[\begin{array}{cc} W_{c1}, & p_1 \end{array}\right]' = h_y(x,w) & \text{Measured Outputs} \\ z & = \left[\begin{array}{cc} F_1, & AFR \end{array}\right]' = h_z(x,w) & \text{Performance Variables} \\ u' & = \left[\begin{array}{cc} EGR, & VGT \end{array}\right] & \text{Control Inputs} \\ w' & = \left[\begin{array}{cc} W_f, & N \end{array}\right] & \text{External Inputs.} \end{array} \tag{3.1}$$

In the next section, we calculate for a given $w$ the desired steady state point $z^*(w)$, the corresponding control signal $u^*(w) = S_u(w)$, and measurements $y^*(w) = S_y(w)$. We refer to $S_y(w)$ as the setpoint map. It determines the measured outputs that the controller is designed to track in order to keep the performance variables $z$ as close as possible to the desired $z^*(w)$ for all fueling rate levels and engine speeds. We develop a family of linear controllers for $EGR$ and $VGT$ actuators, parameterized by $w_0$, that regulate $z(t)$ to $z^*(w)$ as $w$ varies in a small neighborhood of a nominal operating point defined by $w_0$. These linear controllers are then scheduled to obtain a controller defined over the entire operating region. To design one of these linear controllers, $C$, consider the linearization of the system at a nominal operating point, $w_0$, and its corresponding $u_0 = S_u(w_0)$ and $y_0 = S_y(w_0)$. Let $\delta w$, $\delta u$, $\delta y$, and $\delta z$ denote the deviations of the corresponding variables from their nominal values. Let $P_y(s)$ and $P_z(s)$ denote the transfer function matrices from the input $\delta u$ to the measured outputs $\delta y$ and performance outputs $\delta z$, respectively. Similarly, let $P_{fy}(s)$ and $P_{fz}(s)$ denote the transfer function matrices from the input $\delta w$ to the measured outputs $\delta y$ and performance outputs $\delta z$, respectively. Figure 3 shows the resulting block-diagram of the linearized closed loop system. The controller processes the difference $S_y(w) - S_y(w_0) - \delta y$ and generates commands for $EGR$ and $VGT$ actuators to enable engine operation at the optimum equilibrium with respect to emission requirements.

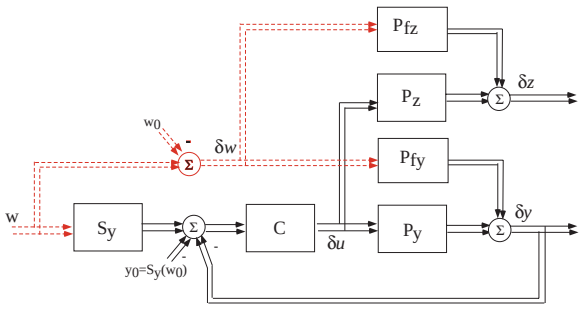


**Figure 3:** Block diagram showing the linearized control problem.

## 4 Steady-State Optimization

The desired steady-state values for the burnt gas fraction and air-to-fuel ratio, $z^*$, are generated using the following procedure. For given $w$ we search for the operating point $u = u^*(w)$ so that $F_1$ is maximized subject to (1.) in-cylinder air-to-fuel ratio, $AFR$, being greater than $\underline{AFR}$ and (2.) intake manifold pressure, $p_1$, being less than $\bar{p}_1$. The first constraint ensures that no visible smoke is generated in steady-state. The lower bound $\underline{AFR}$ can be a function of fueling level and engine speed. For simplicity, however, we assume constant $\underline{AFR} = 25$. The second constraint protects the engine from damage due to high intake manifold pressure (over-boost). We also assume that $\bar{p}_1 = 220$ kPa. The value of $F_1$ is maximized to achieve significant $NOx$ reduction. After selecting the desired setpoints for the performance variables, $z^*$, and its associated inputs, $u^*$, we determine the corresponding measured outputs, $y^*$, using simulation of the engine model.

In Figures 4 to 6 we illustrate the procedure for generating desired setpoints by considering specific external signals, $W_f = 6$ kg/hr and $N = 2500$ rpm. We show how to determine the actuator positions, $EGR^*$ and $VGT^*$, that correspond to maximum $F_1$ for $AFR > \underline{AFR}$. A grid that spans the feasible set for the controller inputs $u$ is selected. The grid is based on the actuator authority, specifically, $EGR$ and $VGT$ vary between 0 and 1 as shown in Figure 4. The significance of the region enclosed by the box in Fig. 4 is explained later in this section. The set of all steady-state points for the performance variables, $z$, that correspond to $W_f = 6$ kg/hr, $N = 2500$ rpm is shown in Figure 5. Similarly, the set of all steady-state points for the measured outputs, $y$, that correspond to $W_f = 6$ kg/hr, $N = 2500$ rpm is shown in Figure 6. The circles indicate the equilibria that satisfy the constraints, the "x"s those that violate the constraints. Our procedure for setpoint generation indicates that $F_1^* = 0.2125$ and $AFR^* = 25.5$ is to be chosen. This setpoint corresponds to the largest value of $F_1$ that is consistent with $AFR$ and $p_1$ satisfying the stated limits.

The $u$ setpoint that generated $F_1^* = 0.2125$ and $AFR^* = 25.5$ is $EGR^* = 0.9$, $VGT^* = 0.1$. The corresponding values of $y$ are $p_1^* = 176.23$ kPa and $W_{c1} = 0.0364$ kg/sec. The optimization has to be repeated for external signals on the selected grid on $w$ and the resulting values of $y^*$ are interpolated to derive the set-point map $S_y$ and $S_u$.

Figures 4 to 6 may be used to demonstrate the two control design issues cited in the Introduction. Consider the second issue first. Suppose we wish to desigh a linear controller to regulate $z$ in the neighborhood of the setpoint $F_1 = 0.2125$ and $AFR = 25.5$. Let us examine the control authority available to do so. The DC gain matrix of the system linearized at this setpoint is given by:

$$\left[\begin{array}{c} \delta F_1 \\ \delta AFR \end{array}\right] = \left[\begin{array}{cc} 0.23 & -0.55 \\ -0.90 & 1.84 \end{array}\right] \left[\begin{array}{c} \delta EGR \\ \delta VGT \end{array}\right] \tag{4.1}$$

The $P_z(0)$ is "almost singular" or "almost rank deficient" in the sense that it has both a large condition number ($\kappa \approx 64$) and a small singular value ($\sigma_{min} \approx 0.04$) [3]. We note that the rank deficiency arises because the two actuators

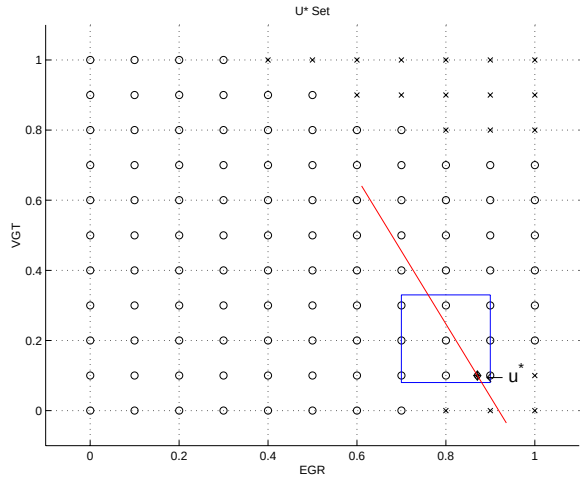


**Figure 4:** Selected grid of control signals for $W_f = 6$ kg/hr and $N = 2500$ rpm.

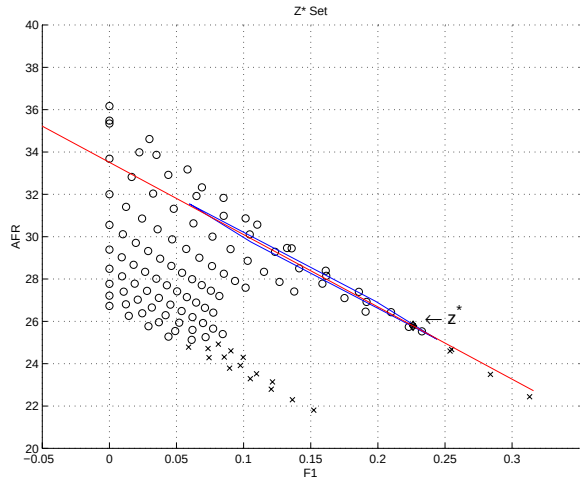


**Figure 5:** Feasible set of performance variables for $W_f = 6$ kg/hr and $N = 2500$ rpm.

have approximately identical effect on the performance variables; i.e., the two columns of $P_z(0)$ are almost collinear. The physical reason for this property is clear: when the burnt gas fraction increases the fresh air charge is displaced from the intake manifold and the in-cylinder air-to-fuel ratio, $AFR$, decreases. We note that the DC gain matrix $P_y(0)$ is relatively well-conditioned, which reflects the fact that EGR and VGT have independent authority to regulate the measured outputs.

The fact that the actuators are locally almost redundant may be illustrated in Figures 4 to 6. Consider how the performance variables change as the actuators move in a small region about the nominal setpoint given in Figure 4. The size of this region in $u$, is chosen so that the nonlinear plant transformations from $u$ to $y$ and $z$ can be approximated with the linear plant transformations $P_y(0)$ and $P_z(0)$. Mapping this set of control commands into the performance and measured outputs gives us the regions shown in Figures 5 and 6. Note that the region in Figures 5 is

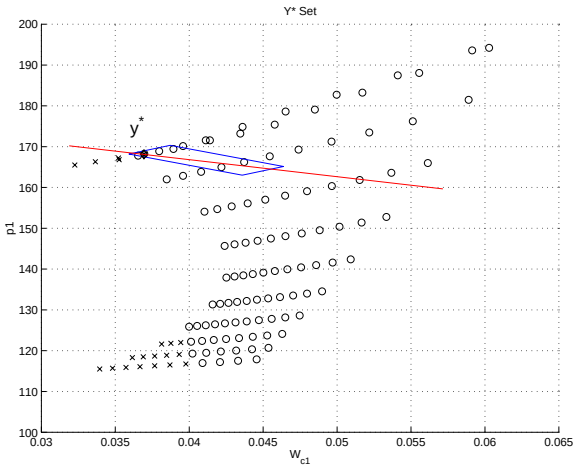


**Figure 6:** Feasible set of measured outputs for $W_f = 6$ kg/hr and $N = 2500$ rpm.

essentially a line in $AFR$ and $F_1$ coordinates. Were the actuators completely redundant, in the sense that they had identical effect on performance variables, this skinny region would reduce to a line similar to the one shown in Figure 5. On the other hand, the region in the $y$ coordinates indicates independent control of the measurements in steady-state by using $EGR$ and $VGT$.

It is important here to mention that the images of the points in the $u$ region lie inside the $z$ region and the $y$ region under the nonlinear mapping, thus showing that the lack of control authority indicated by $P_z(0)$ is indeed present in the actual, nonlinear system. Another important point is that limited control authority coexists with (or is caused by) the maximization of the intake gas burnt fraction, $F_1$. Operating points with less mass burnt fraction, $F_1$, for a given, $AFR$, result in a good condition number for $P_z(0)$.

The other issue cited in the Introduction can now also be seen. Small errors in the steady-state scheduling scheme that correspond to $z^*$ outside the skinny set will result in $y^*$ set points outside the feasible set of $W_{c1}$ and $p_1$. A controller that enforces $y(t)$ to converge to $y^*$ using high gain in both $EGR$ and $VGT$ actuators will cause saturation of both actuators.

## 5 Feedback Controller

The feedback controller must ensure that the engine operates with optimal $F_1$ and $AFR$. The optimum region is narrow and close to the infeasible region of operation. On the other hand, the set-point generation entails large errors due to model uncertainty and numerical interpolations. Thus, there is a large probability for infeasible set-points $z^*$. Any high gain feedback controller (in both actuators) will attempt to track both feasible and infeasible commands using control signals $u^* = P_z(0)^{-1} z^*$.

To address these issues, our control algorithm is designed to coordinate the actuators to achieve maximum authority

and to reduce the impact of strategy errors by not attempting to track infeasible setpoints. These goals are achieved by analyzing the directional properties of the plant using the singular value decomposition of the plant DC gain matrix. This analysis identifies the effective range of the plant, which determines the set of setpoints that may be tracked without incurring excessively large control signals, and the effective rowspace of the plant, which determines how the actuators should be coordinated to achieve maximum authority.

Consider the singular value decomposition (SVD) of $P_z(0)$:

$$P_z(0) = \bar{\sigma}\bar{u}\bar{v}^T + \underline{\sigma}\underline{u}\underline{v}^T \tag{5.1}$$

where $\bar{\sigma} \geq \underline{\sigma}$ are the largest and smallest singular values of $P_z(0)$, and $(\bar{u}, \underline{u})$ and $(\bar{v}, \underline{v})$ are the corresponding sets of left and right singular vectors, respectively. Suppose temporarily that $P_z(0)$ were rank deficient, so that $\underline{\sigma} = 0$. Then it is not possible to track an arbitrary setpoint command; the set of commands that can be tracked is given by the range, or columnspace, of $P_z(0)$, $\mathbf{R}(\mathbf{P_z(0)}) = \mathbf{R}(\bar{\mathbf{u}})$. For our problem, $P_z(0)$ is "almost" rank deficient, in the sense that $0 \ll \underline{\sigma} \ll 1$. It follows that certain commands can be tracked *only* by using large control inputs. To see this, consider a command $z^*$, together with the corresponding steady state control signal $u^*$. Using the SVD, we have that

$$u^* = (1/\sigma_1)\,\bar{v}\bar{u}^T z^* + (1/\sigma_2)\,\underline{v}\underline{u}^T z^*. \tag{5.2}$$

Hence if $z^* = \alpha\underline{u}$ for some $\alpha$, then $\|u^*\| = (1/\sigma_2)\,\|z^*\| \gg \|z^*\|$. It follows that relatively small commands may result in large control signals. On the other hand, commands that satisfy $z^* \in \mathbf{R}(\bar{\mathbf{u}})$ may be tracked without using large control signals; we say that such commands lie in the "effective range" of the plant. A controller with an integrator for each control input will thus achieve perfect steady state tracking of all commands at the expense of large control signals, which are undesirable because they may result in actuator saturation. Although saturation isn't necessarily bad, it is difficult to analyze for systems with multiple actuators and strong interactions. Similar comments apply to controllers whose DC gain is finite but very large.

To avoid potential difficulties with large control signals, we propose a controller of the form $C(s) = G_z K_C(s) H_y$, where $G_z \in \mathbf{R}^{\mathbf{2\times 1}}$ and $H_y \in \mathbf{R}^{\mathbf{1\times 2}}$ are constant unit vectors and $K_C(s)$ is a PI controller (Figure 7). We choose $H_y$ so that the controller attempts to track only those $y$-commands that correspond to $z$-commands that lie in the effective range of $P_z(0)$:

$$H_y = H_z P_z(0) P_y^{-1}(0) / \|H_z P_z(0) P_y^{-1}(0)\|, \tag{5.3}$$

where $H_z = \bar{u}^T$. The transfer function mapping $y$-commands to the control signal in Figure 7 is given by $C(s)\,(I + P_y(s)C(s))^{-1}$, and has DC gain of magnitude $\|G_z H_y\|/|H_y P_y(0) G_z| = \|H_z P_z(0) P_y^{-1}(0)\|/|H_z P_z(0) G_z|$. Because $H_z P_z(0) G_z = \bar{\sigma}\bar{v}^T G_z$, it is easy to verify that choosing $G_z = \bar{v}$ minimizes the size of the steady state control signal. For illustration in Fig. 4 we show the line on which the actuator signals lie as specified by $G_z = \bar{v}$. Similarly, the line in Fig. 5 shows the direction $P_z(0)G_z$ and the line in Fig. 6 shows the direction $P_y(0)G_z$.

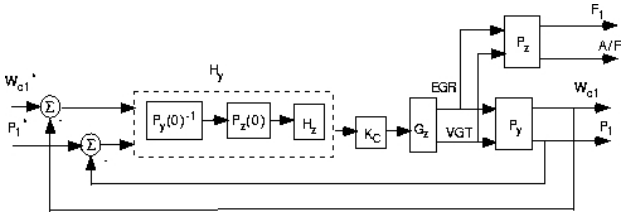


**Figure 7:** Linear feedback controller.

The differences between a two integrator controller and the single integrator controller, $C(s) = G_z K_c(s) H_y$, can be demonstrated by simulating the linearized model. The controller with two integrators was designed so that asymptotic tracking of the set-points by the measured outputs is enforced, and by applying the LQG control design methodology to the augmented plant. The PI controller for the SISO plant $H_y P_y G_z$ was tuned to achieve satisfactory response without violating bandwidth constraints imposed by the cut-off frequency of the actuator. The responses of the two controllers to fuel steps between the levels $6, 5.5, 5.0, 7.0, 7.5, 8.0, 8.5, 7.0, 6.0$ kg/hr at 2500 rpm are shown in Figure 8. We observe that the single integrator controller requires less actuator position deviations from their nominal positions, and while strict tracking of the measured outputs ($W_{c1}$ and $p_1$) is not enforced, the deterioration in the values of performance outputs ($F_1$ and $AFR$) is very small. For example, at $t = 10$ seconds the two integrator controller closes $VGT$ beyond its physical limits (limits were not enforced in this linear simulation) while the single integrator controller closes $VGT$ ls -l only to about 0.02. This results in an error of about 15 kPa in $p_1$ tracking which translates only to very small performance output errors. Smaller actuator effort inherent to the operation of the single integrator controller makes actuator saturation and loss of linear performance associated with actuator saturation and antiwindup less frequent.

The experimental test of the single integrator controller was done in a Visteon's engine dynomometer in Dunton, UK. dSPACE rapid prototyping environment was used to test the controller. The matrices $G_z$ and $H_y$ were gain-scheduled depending on engine speed and fueling rate, the desired steady-state positions of EGR and VGT were used as a feed-forward and the controller $K_c$ was designed as a PI controller where its two gains (proportional and integral) were tuned on the engine. To handle actuator saturation we added an antiwindup that would limit the contribution of the integral term of $K_c$ to a certain value and would stop updating the integrators when saturation is encountered. The setpoint map generates the desired measured outputs shown with dotted line in the first column of plots in Figure 9. The controller generated the desired positions for $VGT$ and $VGT$ actuators that would be passed as setpoints to the inner loop controllers for each of the actuators. The measured outputs and the control signals to fuel steps between levels $2.0, 5.0, 6.0, 5.0, 2.0$ kg/hr are shown in Figure 9. The performance outputs $AFR$ and $F_1$ were not measured directly but estimated by post-processing experimental data.

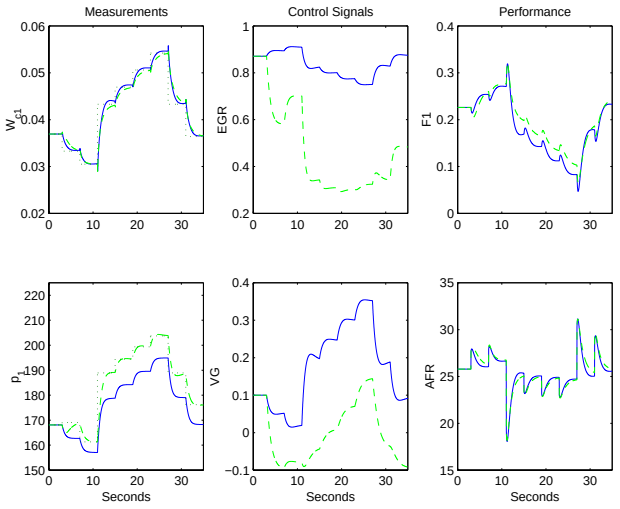


**Figure 8:** Simulation response of the two integrator (dashed) and the single integrator (solid) controllers. The setpoints are indicated by the dotted line.

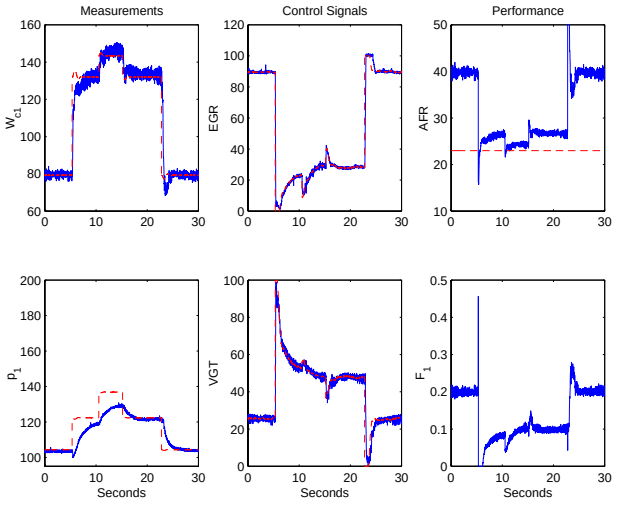


**Figure 9:** Experimental controller response to fuel steps.

## 6 Conclusions

In this paper we formulated an emission reduction control problem for a CIDI engine. We demonstrated that the performance variables cannot be controlled independently using $EGR$ and $VGT$ actuators at the optimal operating points. The plant singularity at the optimal operating points leads to a difficult control problem. We designed a gain scheduled multivariable controller that enables engine operation at the optimal operating points by coordinating $EGR$ and $VGT$ to achieve maximum authority. By simulations and experiments we demonstrated that the closed loop response is robust to strategy errors and it achieves tracking of the performance set points thereby reducing $NO_x$ and smoke emission generation. The complete details of the controller development and the analysis of its robustness properties will be reported elsewhere.

## 7 Acknowledgment

We acknowledge Michiel van Niewstadt, Paul Moraal (Ford Forshugszentrum Aachen, Germany), Paul Wood, Mike Criddle and Mick Campbell (Visteon, Dunton, UK) for establishing appropriate experimental facilities that made the controller evaluation possible. We also thank Jeff Cook, Mrdjan Jankovic (Ford Motor Co., USA), and Rick Middleton (Univ. of Newcastle, Australia) for useful discussions.

## References

[1] Amstutz, A., and Del Re, L.R., "EGO sensor based robust output control of EGR in diesel engines," *IEEE Transactions on Control System Technology,* vol. 3, no. 1, 1995.

[2] J. S. Freudenberg and R. Middleton, "Design Rules for Multivariable Systems," Proc. Conf. on Decision and Control, Japan, 1996.

[3] G. H. Golub and C. F. van Loan, *Matrix Computations,* The Johns Hopkins University Press.

[4] Heywood, J.B., *Internal Combustion Engine Fundamentals*, McGraw-Hill, Inc., 1988.

[5] Kao, M., and Moskwa, J.J., "Turbocharged diesel engine modeling for nonlinear engine control and estimation," *ASME Journal of Dynamic Systems, Measurement and Control*, Vol. 117, 1995.

[6] Kolmanovsky, I., Moraal, P., van Nieuwstadt, M., and Stefanopoulou, A., "Issues in modelling and control of intake flow in variable geometry turbocharged engines," *Proceedings of 18th IFIP Conference on System Modelling and Optimization, Detroit, July 1997*, to appear.

[7] Moody, J.F., "Variable geometry turbocharging with electronic control," *SAE paper No. 860107*, 1986.

[8] M. Morari and E. Zafiriou, *Robust Process Control,* Prentice Hall, 1990.

[9] van Nieuwstadt M., Moraal, P., Kolmanovsky, I., and Stefanopoulou, A., "A comparison of SISO and MIMO designs for EGR-VNT control of a light duty Diesel engine," *Proceedings of IFAC Workshop on Advanced in Automotive Control*, Mohican State Park, Ohio, February 1998.

[10] Porter, B., Ross-Martin, T.J., and Truscott, A.J., "Control technology for future low emissions diesel passenger cars," *Proceedings of the Institution of Mechanical Engineers*, paper C517/035, 1996.

[11] S. Skogestad and I. Postlethwaite, *Multivariable Feedback Control,* John Wiley & Sons, 1996

[12] Tsai, S.-C., Goyal, M.R., "Dynamic turbocharged diesel engine model for control analysis and design," SAE paper No. 860455, 1986.

[13] Watson, N., and Janota, M.S., *Turbocharging the Internal Combustion Engine*, Wiley Interscience, New York, 1982.

[14] Yanakiev, D., and Kanellakopoulos, I., "Engine and transmission modelling for heavy-duty vehicles," *PATH Technical Note 95-6*, 1995.